Control Engineering Practice 19 (2011) 380–394

Contents lists available at ScienceDirect

Control Engineering Practice

journal homepage: www.elsevier.com/locate/conengprac

Gain-scheduling control of port-fuel-injection processes

Andrew White [a], Jongeun Choi [a,b,*], Ryozo Nagamune [c], Guoming Zhu [a,b]

[a] Department of Mechanical Engineering, Michigan State University, United States
[b] Department of Electrical and Computer Engineering, Michigan State University, United States
[c] Department of Mechanical Engineering, University of British Columbia, Canada

ARTICLE INFO

Article history:
Received 16 October 2009
Accepted 7 December 2010
Available online 28 December 2010

Keywords:
Engine control
Port fuel injection
Gain-scheduling control
Linear parameter varying system
LMI optimization

ABSTRACT

An event-based sampled discrete-time linear system representing a port-fuel-injection process based on wall-wetting dynamics is obtained and formulated as a linear parameter varying (LPV) system. The system parameters used in the engine fuel system model are engine speed, temperature, and load. These system parameters can be measured in real-time through physical or virtual sensors. A gain-scheduling controller for the obtained LPV system is then designed based on the numerically efficient convex optimization or linear matrix inequality (LMI) technique. Simulation results show the effectiveness of the proposed scheme.

1. Introduction

Increasing concerns about global climate change and ever-increasing demands on fossil fuel capacity call for reduced emissions and improved fuel economy. Port-fuel-injection (PFI) fuel systems are widely used in vehicles today; however, direct-injection (DI) fuel systems have also been introduced to markets globally. To improve the full load performance of DI engines at high speed, Toyota introduced an engine with a stoichiometric DI system with a DI injector and an intake port injector for each cylinder (see Ikoma et al., 2006). The use of gasoline PFI and ethanol DI dual-fuel system to substantially increase gasoline engine efficiency is described by Heywood, Cohn, and Bromberg (2007). This shows that with the introduction of DI fuel systems for the internal combustion engine, PFI fuel systems will remain part of the engine fuel system for improved engine performance, which is the main motivation for revisiting the air-to-fuel ratio control problem for a PFI fuel system.

There have been several fuel control strategies developed for internal combustion engines to improve the efficiency and exhaust emissions. A key development in the evolution was the introduction of a closed-loop fuel injection control algorithm (Rivard, 1973), followed by the linear quadratic control method (Cassidy & Athans, 1980), and an optimal control and Kalman filtering design (Powers, Powell, & Lawson, 1983). Specific applications of A/F ratio control based on observer measurements in the intake manifold were developed by Benninger and Plapp (1991). Another approach was based on measurements of exhaust gas A/F ratio measured by the oxygen sensor and on the throttle position (Onder, 1993). Choi, Hedrick, Kelsey-Hayes, and Livonia (1998) also developed a nonlinear sliding mode control of A/F ratio based upon the oxygen sensor feedback. Continuing research efforts of A/F ratio control include Wang, Yu, Gomm, Page, and Douglas (2006), Alfieri, Amstutz, and Guzzella (2009), and Yildiz, Annaswamy, Yanakiev, and Kolmanovsky (2010). The conventional A/F ratio control for automobiles uses both closed-loop feedback and feed-forward control to have good steady state and transient responses.

For a spark-ignited engine equipped with a port-fuel-injection system, the wall-wetting dynamics are commonly used to model the fuel injection process; and the wall-wetting effects are compensated on the basis of simple linear models that are tuned and calibrated through engine tests. These models are quite effective for an engine operated at steady state or slow transition conditions but they are difficult for fast transient and other special operational conditions, for instance, during engine cold start. One of the approaches to model the wall-wetting dynamics during engine cold start is to describe it using a family of linear models to approximate the system dynamics at different engine cylinder head temperature, speed and load conditions, that is, to translate the fuel system model into a linear parameter varying (LPV) system.

The use of LPV modeling to control the A/F ratio of a port-fuel-injection system has been reported by Genç (2002). An LPV model is developed with manifold absolute pressure, exhaust value closing, and inlet value opening as the time-varying parameters. However, Genç (2002) does not address the issue of engine cold start. Furthermore, all LPV control synthesis methods used by Genç (2002) are based in continuous time, relying on Tustin's (bilinear)

* Corresponding author at: Departments of Mechanical Engineering, and Electrical and Computer Engineering, Michigan State University, United States.
E-mail addresses: whitea23@egr.msu.edu (A. White), jchoi@egr.msu.edu (J. Choi), nagamune@mech.ubc.ca (R. Nagamune), zhug@egr.msu.edu (G. Zhu).

0967-0661/$ - see front matter © 2010 Elsevier Ltd. All rights reserved.
doi:10.1016/j.conengprac.2010.12.007

Nomenclature

English

c	stoichiometric air-to-fuel ratio
e	measurement for control
e_P	measurement for proportional control
e_I	measurement for integral control
$\mathcal{F}_\ell$	lower linear fractional transformation
$\mathcal{F}_u$	upper linear fractional transformation
$G(q)$	transfer function from m_i to m_c
$H(\Theta)$	feed-forward control compensated generalized plant
$\hat{H}(\Theta)$	Taylor series expansion of feed-forward control compensated generalized plant
$I(q)$	integrator
$K(\Theta)$	gain-scheduling feedback controller
$K_f(\Theta)$	feed-forward controller
$L(q)$	low-pass filter
l	pseudo-output
$M_{A_{O_2}d}$	interconnection matrix for the LFT representing A_{O_2d}
$M_{A_{O_2}^{-1}}$	interconnection matrix for the LFT representing $A_{O_2}^{-1}$
$M_{\alpha/\beta}$	interconnection matrix for the LFT for α/β
$M_{1/\beta}$	interconnection matrix for the LFT for $1/\beta$
M_γ	interconnection matrix for the LFT for γ
m_A	mass of the air trapped in the cylinder
m_c	the mass of fuel trapped in the cylinder
m_i	the mass of fuel injected
m_w	the mass of fuel residual on the wall
$P(\Theta)$	generalized plant without feed-forward control
p	pseudo-input
q	forward shift operator
T_D	transport delay
T_{O_2}	time constant of the oxygen sensor
t_s	sample period
u	control input
$\mathcal{V}_i$	the ith vertex of the parameter variation polytope
ν	engine speed (rpm)
$W_1(q)$	weighting function for w_1
$W_2(q)$	weighting function for w_2
w	exogenous input
w_1	represents the deviation $(m_c/m_A - m_c/m_A^0)$
w_2	desired equivalence ratio
w_3	input to the feed-forward controller
$\tilde{w}_1$	unweighted exogenous input for w_1
$\tilde{w}_2$	unweighted exogenous input for w_2
$\tilde{w}_3$	unweighted exogenous input for w_3
x	states of the feed-forward compensated generalized plant
x_{AUG}	states of augmented plant
x_I	integrator state
x_L	low-pass filter state
x_{ww}	wall-wetting state
x_{comb}	combustion state
x_{O_2}	states of the oxygen sensor
y	equivalence ratio
y_s	measured equivalence ratio
z	error output

Greek

α	ratio of fuel delivered from the wall to the cylinder
α_0	nominal value of α
α_δ	time-varying fluctuation of α
β	ratio of the fuel entering the cylinder from injection
β_0	nominal value of β
β_δ	time-varying fluctuation of β
γ	normalized inverse engine speed
η	$\mathcal{H}_\infty$ performance bound
Θ	time-varying parameter structure
λ	barycentric coordinates

State-space realizations (Each state-space realization used in this paper are listed below in order of appearance.)

$\{A_{O_2}, B_{O_2}, C_{O_2}\}$	continuous-time state-space matrices of the oxygen sensor
$\{A_{O_2d}, B_{O_2d}, C_{O_2d}\}$	discrete-time state-space matrices of the oxygen sensor
$\{\hat{A}_{O_2d}, \hat{B}_{O_2d}, \hat{C}_{O_2d}\}$	discrete-time state-space matrices of the oxygen sensor after performing the fourth-order Taylor series approximation
$\{A, B_0, B_1, B_2, C_0, D_{00}, D_{01}, D_{02}, C_1, D_{10}, D_{11}, D_{12}\}$	discrete-time LPV system state-space matrices
$\{\hat{A}, \hat{B}_1, \hat{B}_2, \hat{C}_1, \hat{D}_{11}, \hat{D}_{12}\}$	discrete-time state-space realization after performing first-order Taylor series expansion
$\{A_L, B_L, C_L\}$	low-pass filter state-space realization
$\{\tilde{A}, \tilde{B}_1, \tilde{B}_2, \tilde{C}_1, \tilde{D}_{11}, \tilde{D}_{12}, \tilde{C}_2\}$	augmented discrete-time state-space realization
$\{\overline{A}, \overline{B}_1, \overline{B}_2, \overline{C}_1, \overline{D}_{11}, \overline{D}_{12}, \overline{C}_2\}$	discrete-time polytopic state-space realization

transformation to convert the discrete-time system to a continuous-time system, thus fixing the engine speed and sampling rate of the discrete-time system.

The contribution of this paper is as follows. First, an event-based, discrete-time LPV model for the wall-wetting and oxygen sensor dynamics with wall-wetting parameters and engine speed as scheduling variables is developed. Then an event-based, gain-scheduling controller for the derived LPV model is designed. To cope with practical situations, the discrete-time LPV control synthesis method given by Caigny, Camino, Oliveira, Peres, and Swevers (2008) is used to develop the event-based, gain-scheduling controller.

The control structure used in this study is a proportional-integral (PI) controller. PI controllers are widely used in industry since they are well understood by control engineers. The PI gains are often calibrated in a field test for the best performance as functions of system operational conditions. However, the system stability and performance are not guaranteed for all time-varying parameters. Therefore, LPV techniques are applied to design gain-scheduling PI controllers for guaranteed stability and performance for all time-varying parameters, which is expected to be well received by industrial control engineers.

The paper is organized as follows. The models and the modeling techniques used in this paper are given in Section 2. The design of the gain-scheduling controller in Section 3 is covered by first introducing the control strategy in Section 3.1. Then the feed-forward compensated generalized plant is developed in Section 3.2 and its first-order Taylor series expansion is computed in Section 3.3. Next the measurement for control is elaborated in Section 3.4. The gain-scheduling synthesis problem is stated in Section 3.5. In Section 3.6, the augmented LPV plant obtained in Section 3.4 is converted into a polytopic time-varying system, which is an LPV system with a polytopic dependency on a scheduling parameter that takes values in the unit-simplex, so that the gain-scheduling controller synthesis technique given by Caigny et al. (2008) can be performed. For comparison, a linear time-invariant feedback $\mathcal{H}_\infty$

controller is designed in Appendix A.5 using the nominal parameters. Simulation results from three separate engine operating conditions are presented in Section 4. A summary is presented in the final section.

Standard notation is used throughout the paper. Let $\mathbb{R}, \mathbb{Z}$ and $\mathbb{Z}_{\geq 0}$ denote, respectively, the set of real, integer, and non-negative integer numbers. The positive definiteness of a matrix A is denoted by $A \succ 0$. The maximum (respectively, minimum) of α is denoted by $\overline{\alpha}$ (respectively, $\underline{\alpha}$). The abbreviation LFT is used to denote a linear fractional transformation, which is described in Appendix A.1. Furthermore, a lower (respectively, upper) LFT is denoted by $\mathcal{F}_\ell$ (respectively, $\mathcal{F}_u$). The ℓ_2 space of square-summable sequences on the set of non-negative integers $\mathbb{Z}_{\geq 0}$ is given by

$$\ell_2 := \left\{ x : \mathbb{Z}_{\geq 0} \to \mathbb{R}^n \middle| \sum_{k=0}^{\infty} x^T(k)x(k) < \infty \right\}.$$

For a signal x in the ℓ_2 space, its ℓ_2 norm is defined as

$$\|x\|_{\ell_2} := \left(\sum_{k=0}^{\infty} x^T(k)x(k) \right)^{1/2}.$$

Other notation will be explained in due course.

2. Event-based discrete-time system modeling

In this section, the dynamics of the plant (Fig. 1) will be carefully explained and modeled to develop a control oriented linear parameter varying (LPV) model. The plant given in Fig. 1 shows the port-fuel-injection process for a single cylinder engine. However, the methods used in this paper can be extended to a multiple cylinder engine by using the individual cylinder fuel–gas ratio estimation method developed by Suzuki, Shen, Kako, and Oguri (2007).

2.1. Sampling period of the event-based discrete-time system

The discrete-time linear system is obtained by event-based sampling of the port-fuel-injection process; hence the sampling time of this discrete-time system is the period of an engine cycle,

$$t_s = \frac{1\,\text{min}}{v\,\text{rev}} \left(\frac{60\,\text{s}}{1\,\text{min}} \right) \left(\frac{2\,\text{rev}}{1\,\text{cycle}} \right) = \frac{120}{v} \frac{\text{s}}{\text{cycle}}, \tag{1}$$

where v represents the engine speed in revolutions per minute (rpm) (see general engine modeling techniques in Balluchi et al., 2000).

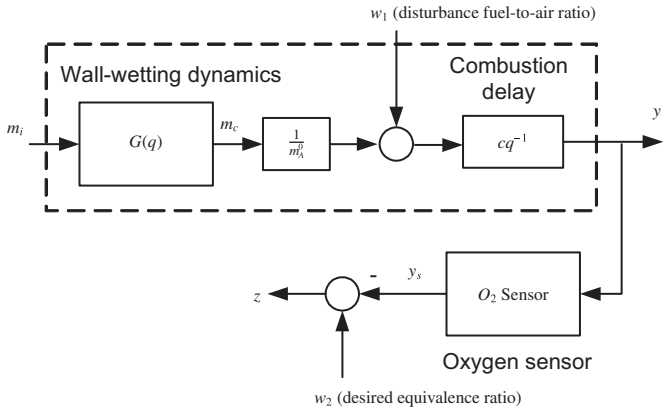

Fig. 1. The block diagram of the port-fuel-injection process and sensor dynamics.

2.2. Dynamics of the port-fuel-injection process

The wall-wetting dynamics can be described as follows:

$$\begin{aligned} m_w(k) &= (1-\alpha_k)m_w(k-1) + (1-\beta_k)m_i(k), \\ m_c(k) &= \alpha_k m_w(k-1) + \beta_k m_i(k), \end{aligned} \tag{2}$$

where $k \in \mathbb{Z}_{\geq 0}$, and m_w, m_c, and m_i denote the amount of fuel, on the wall, in the cylinder, and injected, respectively. The coefficients $\alpha \in [0,1]$ and $\beta \in [0,1]$ are the ratios of the fuel delivered from the wall to the cylinder, and of the fuel entering the cylinder from injection, respectively. For notational simplicity, α_k and β_k will be used to denote the wall-wetting parameters at time k, such that $\alpha_k = \alpha(k)$ and $\beta_k = \beta(k)$. These values can be estimated online through an available set of engine sensors, which allows the application of gain-scheduling control to the plant. Using the discrete-time dynamics in (2), the transfer function $G(q)$ from m_i to m_c is

$$G(q) := \frac{m_c(k)}{m_i(k)} = \frac{\beta_k + (\alpha_k - \beta_k)q^{-1}}{1-(1-\alpha_k)q^{-1}}, \tag{3}$$

where q is the *forward shift operator* that satisfies $qu(k) = u(k+1)$. The dotted box in the block diagram in Fig. 1 illustrates the fuel-injection process. The output of $G(q)$ is the input to the gain block of $1/m_A^0$, which is the nominal value of the inverse of the mass of air trapped in the cylinder m_A. The signal w_1 represents the deviation $(m_c/m_A - m_c/m_A^0)$, which will be treated as a disturbance in this paper. Another constant gain factor $c = 14.6$ in Fig. 1 is the value for the air-to-fuel-ratio at stoichiometric. After the combustion delay block the equivalence ratio y is generated. The diagram of the transfer function from the amount of fuel injected m_i and the disturbance w_1 to the equivalence ratio y (inverse of normalized air-to-fuel ratio) is shown in the dotted box in Fig. 1.

2.3. Dynamics of the oxygen sensor

To measure y, a full range oxygen sensor is placed in the exhaust manifold at some distance downstream from the exhaust valve. Notice that the continuous-time dynamics and delays will change in the event-based, discrete-time system according to the speed of the engine (or the sampling time). Therefore, the objective of this section is to obtain oxygen sensor dynamics in the form of a finite dimensional, event-based, discrete-time LPV system. Finite dimensionality is required to apply most LPV controller design techniques and the controller design method which will be presented in Section 3. To this end, in general, one can approximate the continuous-time system with a delay by a finite dimensional event-based, discrete-time LPV system in any standard method. To illustrate this procedure, we demonstrate how we approximate the oxygen sensor dynamics by Taylor series approximation in which the approximation error can be minimized by increasing the order of the Taylor series approximation.

The dynamics of the oxygen sensor are modeled as a first-order sensor delay coupled with the transport delay of the exhaust gas mixture. The transport delay, $T_D = d/v$, of the exhaust gas mixture is both a function of the oxygen sensor placement, which determines the constant d, and the engine speed, v. The combined transfer function in the continuous time domain is

$$y_s(s) = \frac{\exp(-T_D s)}{T_{O_2} s + 1} y(s), \tag{4}$$

where y_s is the equivalence ratio measured by the sensor and T_{O_2} is the time constant of the oxygen sensor. Since the delay $T_D \in [d/\overline{v}, d/\underline{v}]$ is small, Eq. (4) can be approximated by the second-order

system

$$y_s(s) = \frac{1}{T_D s+1}\frac{1}{T_{O_2} s+1} y(s),$$

which has the state-space representation

$$\dot{x}_{O_2} = \underbrace{\begin{bmatrix} -\frac{1}{T_D} & \frac{1}{T_D} \\ 0 & -\frac{1}{T_{O_2}} \end{bmatrix}}_{=A_{O_2}} x_{O_2} + \underbrace{\begin{bmatrix} 0 \\ \frac{1}{T_{O_2}} \end{bmatrix}}_{=B_{O_2}} y,$$

$$y_s = \underbrace{[1 \;\; 0]}_{=C_{O_2}} x_{O_2}. \tag{5}$$

Using t_s as the sampling rate, the corresponding discrete system of Eq. (5) is

$$x_{O_2}(k+1) = A_{O_2 d} x_{O_2}(k) + B_{O_2 d} y(k),$$

$$y_s(k) = C_{O_2 d} x_{O_2}(k), \tag{6}$$

where, due to the invertibility of the matrix A_{O_2} in (5),

$$A_{O_2 d} = \exp(A_{O_2} t_s),$$

$$B_{O_2 d} = \left(\int_0^{t_s} \exp(A_{O_2}\tau)\, d\tau\right) B_{O_2} = A_{O_2}^{-1}(A_{O_2 d} - I) B_{O_2},$$

$$C_{O_2 d} = C_{O_2}.$$

Since both T_D and t_s are functions of engine speed, v, naturally $A_{O_2 d}$ and $B_{O_2 d}$ are as well. A fourth-order Taylor series approximation is used to capture the parameter variation of $A_{O_2 d}$. To ensure that the coefficients of the Taylor series approximation of $A_{O_2 d}$ are numerically stable, the engine speed, v, can be normalized. Furthermore, due to the way that v appears in $A_{O_2}^{-1}$, it is useful to isolate $1/v$ instead of v. For this reason, the inverse of the engine speed $1/v \in [1/\overline{v}, 1/\underline{v}]$ is normalized to γ in the following way:

$$\gamma = \frac{\frac{1}{v} - \frac{1}{v_0}}{\frac{1}{v} + \frac{1}{v_0}} \quad \text{where} \quad \frac{1}{v_0} = \frac{\frac{1}{\overline{v}} + \frac{1}{\underline{v}}}{2}. \tag{7}$$

The polynomial LFTs (Zhou, Doyle, & Glover, 1996 Chap. 10) $M_{A_{O_2 d}}$ and $M_{A_{O_2}^{-1}}$ are used to isolate the varying parameter γ. The details for the computation of the polynomial LFTs $M_{A_{O_2 d}}$ and $M_{A_{O_2}^{-1}}$ are provided in Appendix A.2.

The approximated state-space matrices $\hat{A}_{O_2 d}$ and $\hat{B}_{O_2 d}$ are represented in Fig. 2 by their respective dotted boxes. The approximated state matrix $\hat{A}_{O_2 d}$ block is formed by the lower LFT $M_{A_{O_2 d}}$ connected to the time-varying parameter matrix $\gamma_k I_4$ (for details, see Appendices A.1 and A.2). The approximated input matrix $\hat{B}_{O_2 d}$ block is formed by the matrix multiplications of $B_{O_2 d}$ in Eq. (6). The $\hat{A}_{O_2 d}$, $\hat{B}_{O_2 d}$, and $C_{O_2 d}$ blocks are then connected in the standard state-space interconnection (Skogestad & Postlethwaite, 2005). After performing the interconnection displayed in Fig. 2, the fourth-order approximated system used for controller design is given by

$$\hat{x}_{O_2}(k+1) = \hat{A}_{O_2 d}(\gamma_k)\hat{x}_{O_2}(k) + \hat{B}_{O_2 d}(\gamma_k) y(k),$$

$$\hat{y}_s(k) = C_{O_2 d}\hat{x}_{O_2}(k), \tag{8}$$

where, with calculations presented in Appendix A.2, we can derive

$$\hat{A}_{O_2 d}(\gamma_k) = \begin{bmatrix} \exp(-\frac{120}{d}) & a(\gamma_k) \\ 0 & b(\gamma_k) \end{bmatrix},$$

$$\hat{B}_{O_2 d}(\gamma_k) = \begin{bmatrix} \frac{d(\gamma_k+1)}{v_0(\gamma_k-1)}\left(\frac{a(\gamma_k)}{T_{O_2}}\right) - b(\gamma_k) + 1 \\ 1 - b(\gamma_k) \end{bmatrix}.$$

The following polynomial functions $a(\gamma_k)$ and $b(\gamma_k)$:

$$a(\gamma_k) = 0.3972 - 0.4891\gamma_k - 0.0984\gamma_k^2 + 0.0608\gamma_k^3 + 0.0975\gamma_k^4,$$

$$b(\gamma_k) = 0.3114 - 0.7266\gamma_k + 0.1211\gamma_k^2 + 0.3095\gamma_k^3 + 0.2231\gamma_k^4,$$

were found when selecting an oxygen sensor time constant of $T_{O_2} = 0.06$ s and a transport delay of $T_D = 80/v$, by setting $d = 80$, indicating that the transport delay is about 54 ms at an engine speed of 1500 rpm. This was determined empirically through engine calibration tests.

To demonstrate the effectiveness of the proposed model for the event-based sampling of the oxygen sensor delay, a comparison is made between the proposed fourth-order Taylor series approximation model and a fixed model computed at the nominal engine speed (3500 rpm). In Fig. 3, the step response of the fourth-order Taylor series approximation model (dashed line) is compared to the exact discretized model (solid line) at engine speeds of 1000 and 6000 rpm. The fixed model computed at the nominal engine speed (dash-dot line) is also compared to the exact model in Fig. 3. It is clear that the fixed model computed at the nominal engine speed either responds too slowly when the engine speed is less than the nominal speed or too quickly when the engine speed is greater than the nominal speed. However, the approximated model's response very closely follows the exact model's response as shown in Fig. 3.

2.4. An LPV system

In summary, by combining the wall-wetting dynamics in (2) and the oxygen sensor delay and dynamics in (8) as shown in Fig. 1, we obtain the following LPV system for the event-based discrete-time

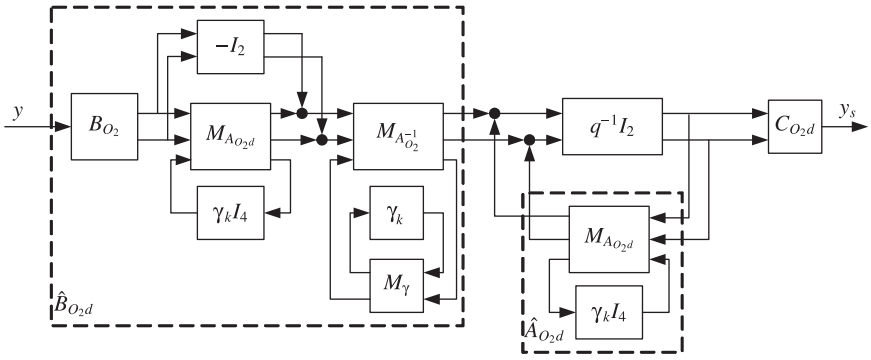

Fig. 2. Block diagram of the combined dynamics of the exhaust gas and sensor delays.

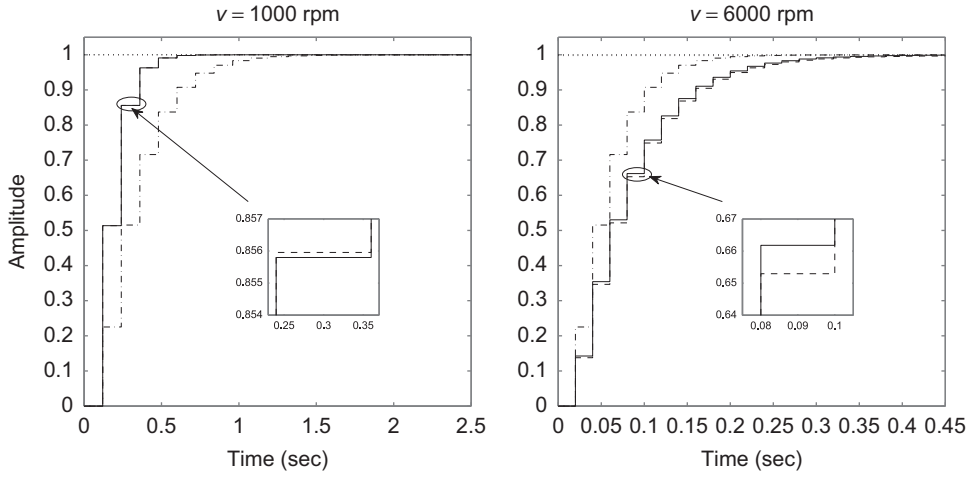

Fig. 3. Comparison of the response to a unit step function for the fourth-order Taylor series approximation model in Eq. (8) (dashed line) and a model equation (6) with the engine speed fixed at 3500 rpm (dash-dot line) to the exact discretized oxygen sensor delay model in Eq. (6) (solid line) at 1000 and 6000 rpm.

Table 1
Modeling parameters.

Parameter	Value used in paper
T_D is a function of engine speed, ν	$\frac{80}{\nu}$
T_{O_2} is a constant	0.06

Table 2
Measurable time-varying parameters (scheduling parameters).

α(cylinder head temperature (t),manifold absolute pressure (t)) $\in$ [0.081,0.1]
β(cylinder head temperature (t),manifold absolute pressure (t)) $\in$ [0.28,0.89]
$\gamma(v(t)) = \frac{\frac{1}{v(t)} - \frac{1}{v_0}}{\frac{1}{v(t)} + \frac{1}{v_0}} \in [-0.55556, 0.26316]$

port-fuel-injection and oxygen sensor dynamics:

$$\begin{bmatrix} x_{ww}(k+1) \\ x_{comb}(k+1) \\ \hat{x}_{O_2}(k+1) \end{bmatrix} = \begin{bmatrix} 1-\alpha_k & 0 & 0 \\ \frac{c\alpha_k}{m_A^0} & 0 & 0 \\ 0 & \hat{B}_{O_2 d}(\gamma_k) & \hat{A}_{O_2 d}(\gamma_k) \end{bmatrix} \begin{bmatrix} x_{ww}(k) \\ x_{comb}(k) \\ \hat{x}_{O_2}(k) \end{bmatrix} + \begin{bmatrix} 1-\beta_k \\ \frac{c\beta_k}{m_A^0} \\ 0 \end{bmatrix} m_i(k) + \begin{bmatrix} 0 \\ c \\ 0 \end{bmatrix} w_1(k),$$

$$z(k) = [0 \;\; 0 \;\; -C_{O_2 d}] \begin{bmatrix} x_{ww}(k) \\ x_{comb}(k) \\ \hat{x}_{O_2}(k) \end{bmatrix} + w_2(k), \tag{9}$$

where $x_{ww}(k) = m_w(k-1)$ and $x_{comb}(k)$ are the wall-wetting state and the combustion state for the system in the dotted box in Fig. 1.

As can be seen from Eqs. (5), (6), (8), and (9), to apply the model of the LPV system, one needs to identify T_D and T_{O_2} (which are shown in Table 1) and measurable time-varying parameters such as α, β, and γ (which are shown in Table 2), which will be used for scheduling the gain of the controller. In particular, the identified bounds of scheduling variables ($[\underline{\alpha},\overline{\alpha}]$,$[\underline{\beta},\overline{\beta}]$ and $[\underline{\gamma},\overline{\gamma}]$) as shown in Table 2 will be used in synthesizing the gain-scheduling controller. From now on, a compact notation Θ will denote an appropriate gain-scheduling matrix that contains the scheduling variables. The specific structure of Θ will be presented in Eq. (14) of Section 3.2. In addition, the LPV system in Eq. (9) is denoted by $P(\Theta)$. In the following section, we illustrate how to design the LPV gain-scheduling controller as a function of Θ for the LPV model developed in this section.

3. LPV gain-scheduling controller design

3.1. Control strategy

The objective of the control system is to regulate the equivalence ratio y to a reference input w_2 using feed-forward and feedback control against the disturbance signal w_1 (see Fig. 1) and the time-varying wall-wetting dynamics. In particular, we want to guarantee the stability of the closed-loop system and also minimize the effect of the disturbances for any conceivable wall-wetting dynamics variations. The proposed control architecture is illustrated in Fig. 4. This scheme has four components, that is a feedback controller $K(\Theta)$, a feed-forward controller $K_f(\Theta)$, a filter $L(q)$, and an integrator $I(q)$.

The feedback controller $K(\Theta)$ will be designed for the generalized plant (solid box of Fig. 4), after selecting $K_f(\Theta)$, $L(q)$, $I(q)$ and weighting functions $W_1(q)$ and $W_2(q)$. Next, we will explain how to select these functions. After the selection, we will derive the generalized plant in Section 3.4 and we will synthesize $K(\Theta)$ for the derived generalized plant in Section 3.5.

The feed-forward controller $K_f(\Theta)$ is designed using the inverse of $cG(q)$

$$K_f(\Theta) = \frac{G^{-1}(q)}{c} = \frac{1}{c}\left(\frac{1-(1-\alpha_k)q^{-1}}{\beta_k+(\alpha_k-\beta_k)q^{-1}}\right).$$

The selection of the inverse of the plant as a feed-forward controller is a standard technique (Skogestad & Postlethwaite, 2005). The input to the feed-forward controller is the mass of the air m_A, which can be measured online, multiplied by the equivalence ratio set point w_2. This is denoted by w_3, such that $w_3 = w_2 m_A$. $L(q)$ is designed as a low-pass filter such that the error output $z(k)$ is filtered with it

$$L(q) = \frac{0.9999}{q-0.0001405}.$$

The reason to filter the error output is that the control synthesis technique given by Caigny et al. (2008) requires that the output

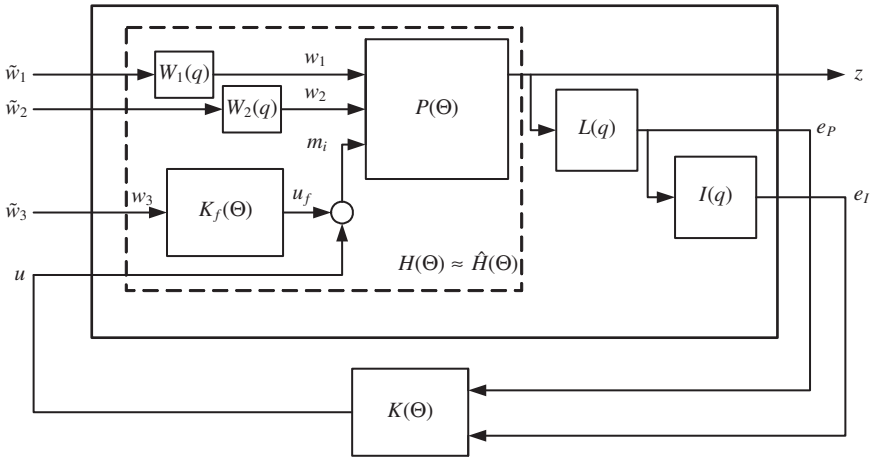

Fig. 4. The proposed control strategy for the fuel injection process (without the weighting functions $W_1(q)$ and $W_2(q)$). Weighting functions $W_1(q)$ and $W_2(q)$ are only used for controller synthesis. A first-order Taylor series expansion is applied to the systems inside the dashed box and the LPV control strategy is applied to all of the systems inside of the bold box.

matrix be independent of the time-varying parameters and the measurement for control must not be corrupted by the unweighted exogenous input, $\tilde{w}(k)$ of the generalized plant. The low-pass filtering for this purpose is a standard procedure (Apkarian, Gahinet, & Becker, 1995). The low-pass filter $L(q)$ was obtained from the discretization of the following first-order continuous transfer function:

$$L^c(s) = \frac{2\pi f_c}{s+2\pi f_c}$$

with a sample period of $120/v_0$. The cut-off frequency f_c of $L^c(s)$ was selected to be 20 Hz, which is high enough to obtain low error between the intended output of the continuous-time filter $L^c(q)$ and the observed output of the discrete-time filter $L(q)$ at different engine speeds, since the sampling rate is engine speed dependent. The filtered output is also integrated using the integrator

$$I(q) = \frac{1}{q-1}$$

to obtain zero steady-state error.

To use ℓ_2 gain or $\mathcal{H}_\infty$ norm (Zhou et al., 1996) for the performance criterion for shaping the frequency response of the closed-loop system, weighing functions (which can be considered design parameters) are also introduced in Fig. 4. The weighting functions are selected in the continuous-time domain as

$$W_1^c(s) = \frac{100}{50s+1},$$

$$W_2^c(s) = \left(\frac{20}{50s+1}\right)^2.$$

The bandwidth (or cut-off frequency) of each weighting function is very small and the DC gain is large, as shown in Fig. 5. The weighting functions are selected to model the frequency content of their respective input. For the fuel-to-air ratio disturbance w_1, the weighting function $W_1^c(s)$ is selected as a simple first-order low-pass filter to place an emphasis on low frequency disturbances, such as a step throttle change. The weighting function $W_2^c(s)$ is chosen to be a second-order low-pass filter with a high DC gain (4 times larger than that of $W_1^c(s)$) to provide more weight on the low frequency signals since w_2 is the step input of the desired equivalence ratio. To incorporate the weighting functions $W_1^c(s)$ and $W_2^c(s)$ into the discrete time system, they were discretized at a sample period of $120/v_0$ to obtain the following discrete-time weighting functions:

$$W_1(q) = \frac{0.1411}{q-0.9986},$$

$$W_2(q) = \frac{0.0003982q+0.0003979}{q^2-1.997178q+0.997180}.$$

The input to each of the weighting functions is the unweighted exogenous inputs which are denoted by $\tilde{w}_1$, $\tilde{w}_2$, and $\tilde{w}_3$. Since there is no weighting function for w_3, in this case $\tilde{w}_3 = w_3$; which means that it is weighted equally at all frequencies. Notice that the weighting functions are chosen by the expected system inputs and their relative (frequency) importance, and they are only used for controller synthesis (Skogestad & Postlethwaite, 2005; Zhou et al., 1996).

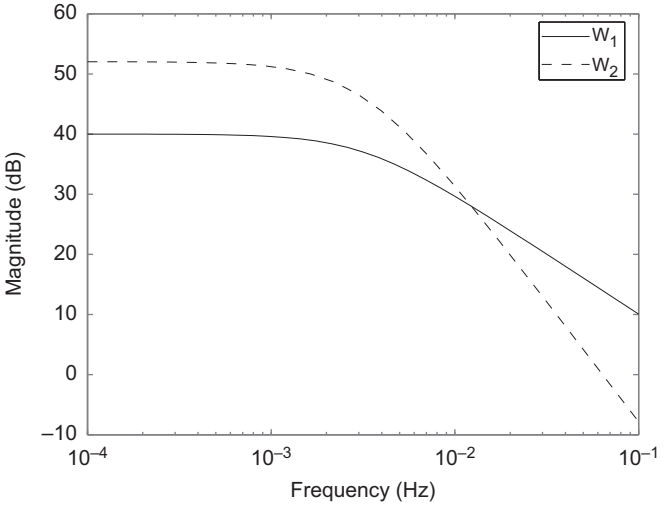

Fig. 5. Magnitude plot of the weighting functions W_1 and W_2.

3.2. Feed-forward compensated generalized plant

The feed-forward compensated generalized plant is denoted by $H(\Theta)$. As depicted in the dashed box of Fig. 4, the feed-forward compensated generalized plant consists of the feed-forward controller $K_f(\Theta)$, the plant $P(\Theta)$, and the weighting functions $W_1(q)$ and $W_2(q)$. The components of the feed-forward controller $K_f(\Theta)$ and the plant $P(\Theta)$ are illustrated in Fig. 6. The feed-forward controller $K_f(\Theta)$ components are encased inside of the dashed box in Fig. 6 and the plant $P(\Theta)$ components are outside of the dashed box.

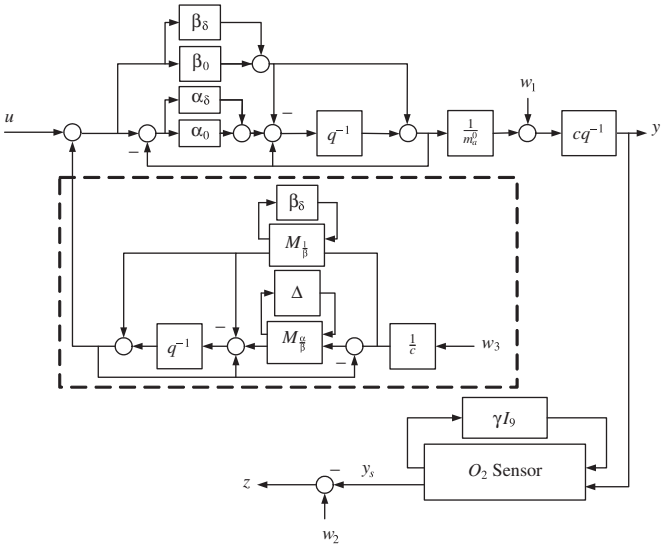

Fig. 6. The feed-forward control compensated generalized plant with the time-varying parameters included.

In the feed-forward control compensated generalized plant $H(\Theta)$, the time-varying parameters α_k and β_k are equivalently transformed to a constant nominal value plus a time-varying fluctuation. For instance, the parameter variation of $\alpha_k \in [\underline{\alpha},\overline{\alpha}]$ with $\alpha_0 = (\underline{\alpha}+\overline{\alpha})/2$ is represented by

$$\alpha_\delta(k) = \alpha_k - \alpha_0 \in [\underline{\alpha}-\alpha_0, \overline{\alpha}-\alpha_0],$$

so that the parameter range of $\alpha_\delta(k)$ is centered around zero. Hence, α_k is replaced by $\alpha_0+\alpha_\delta(k)$. The same is done for $\beta_k \in [\underline{\beta},\overline{\beta}]$ as well. The parameter variation of v is represented by γ as shown in Eq. (7). The upper LFTs (see Appendix A.1) inside the dotted box in Fig. 6, $M_{1/\beta}$ and $M_{\alpha/\beta}$ are used to isolate the time-varying parameters $\beta_\delta(k)$ and $\alpha_\delta(k)$ (Zhou et al., 1996, Chap. 10). β_δ is isolated from $1/\beta_k$ by

$$\frac{1}{\beta_k} = \frac{1}{\beta_0+\beta_\delta(k)} = \mathcal{F}_u(M_{1/\beta},\beta_\delta(k)), \tag{10}$$

where

$$M_{\frac{1}{\beta}} = \left[\begin{array}{c|c} -\frac{1}{\beta_0} & -\frac{1}{\beta_0} \\ \hline \frac{1}{\beta_0} & \frac{1}{\beta_0} \end{array}\right]. \tag{11}$$

Both $\beta_\delta(k)$ and $\alpha_\delta(k)$ are isolated from α_k/β_k by

$$\frac{\alpha_k}{\beta_k} = \frac{\alpha_0+\alpha_\delta(k)}{\beta_0+\beta_\delta(k)} = \mathcal{F}_u(M_{\alpha/\beta},\Delta(k)), \tag{12}$$

where

$$M_{\frac{\alpha}{\beta}} = \left[\begin{array}{cc|c} -\frac{1}{\beta_0} & -\frac{1}{\beta_0} & -\frac{\alpha_0}{\beta_0} \\ 0 & 0 & 1 \\ \hline \frac{1}{\beta_0} & \frac{1}{\beta_0} & \frac{\alpha_0}{\beta_0} \end{array}\right], \quad \text{and} \quad \Delta(k) = \left[\begin{array}{cc} \beta_\delta(k) & 0 \\ 0 & \alpha_\delta(k) \end{array}\right].$$

With the parameter variation represented in this way, the system is written as a discrete-time LPV system with LFT parameter dependency,

$$\begin{bmatrix} x(k+1) \\ l(k) \\ z(k) \end{bmatrix} = \begin{bmatrix} A & B_0 & B_1 & B_2 \\ C_0 & D_{00} & D_{01} & D_{02} \\ C_1 & D_{10} & D_{11} & D_{12} \end{bmatrix} \begin{bmatrix} x(k) \\ p(k) \\ \tilde{w}(k) \\ u(k) \end{bmatrix},$$

$$p(k) = \Theta(k) l(k), \tag{13}$$

where $x(k) \in \mathbb{R}^n$ is the state at time k, $\tilde{w}(k) \in \mathbb{R}^r$ is the unweighted exogenous input, $z(k) \in \mathbb{R}^p$ is the error output, $p(k), l(k) \in \mathbb{R}^{n_p}$ are the pseudo-input and pseudo-output connected by $\Theta(k)$, and $u(k) \in \mathbb{R}^m$ is the control input. The state-space matrices for the LPV system in (13) are provided in (41) of Appendix A.3.

The time-varying parameter Θ in Eq. (13) follows the structure

$$\Theta \in \mathbf{\Theta} = \{\text{diag}\,(\beta_\delta I_3, \alpha_\delta I_2, \gamma I_9) : |\alpha_\delta| \le \delta_1, |\beta_\delta| \le \delta_2, |\gamma| \le 1\}, \tag{14}$$

where $\delta_1 = (\overline{\alpha}-\underline{\alpha})/2$ and $\delta_2 = (\overline{\beta}-\underline{\beta})/2$.

3.3. First-order Taylor series expansion of the LPV system

By inspection of the LPV system in Eq. (13), D_{00} was found to be a non-zero matrix. Hence, the system matrices are not affine functions, i.e., a linear combination of the time-varying parameters plus a constant translation. It is noted at this juncture that LPV control techniques exist which do handle rational parameter variation, namely the method developed by Wu and Dong (2006). However, for discrete-time systems, no controller formula covering all parameter variation is given by Wu and Dong (2006). Instead, for each set of parameters a controller must be solved for using the method given by Gahinet (1996). Since a different controller is needed for each set of parameters, gridding over the parameter space (Apkarian & Adams, 1998) is necessary, which increases the complexity of implementing the controller in practice. In contrast, the method developed by Caigny et al. (2008) does not require any gridding over the parameter space. Also, as shown in Eq. (14) and Table 2 each of the parameters are less than 1 at all times. Therefore, neglecting the higher-order parameter variation is a justifiable approximation. Hence, to utilize the control synthesis technique given by Caigny et al. (2008), we calculate the first-order Taylor series approximation of the system matrices to obtain affine functions in Θ. To find the Taylor series expansion, first the LFT (13) is re-arranged to the following representation:

$$\begin{bmatrix} l(k) \\ x(k+1) \\ z(k) \end{bmatrix} = \underbrace{\left[\begin{array}{c|ccc} D_{00} & C_0 & D_{01} & D_{02} \\ \hline B_0 & A & B_1 & B_2 \\ D_{10} & C_1 & D_{11} & D_{12} \end{array}\right]}_{=:M} \begin{bmatrix} p(k) \\ x(k) \\ \tilde{w}(k) \\ u(k) \end{bmatrix},$$

$$p(k) = \Theta(k) l(k). \tag{15}$$

Notice that Eq. (15) is an upper LFT, i.e.,

$$\begin{aligned} H(\Theta) &:= \mathcal{F}_u(M,\Theta) \\ &= \begin{bmatrix} A & B_1 & B_2 \\ C_1 & D_{11} & D_{12} \end{bmatrix} + \begin{bmatrix} B_0 \\ D_{10} \end{bmatrix} \Theta (I - D_{00}\Theta)^{-1} [C_0 \;\; D_{01} \;\; D_{02}]. \end{aligned} \tag{16}$$

Using the Taylor series expansion at $\Theta = 0$, the system can be approximated as

$$\begin{aligned} \hat{H}(\Theta) &= H(0) + \alpha_\delta[\nabla_{\alpha_\delta} H(0)] + \beta_\delta[\nabla_{\beta_\delta} H(0)] + \gamma[\nabla_\gamma H(0)], \\ &=: \begin{bmatrix} \hat{A}(\alpha_\delta,\beta_\delta,\gamma) & \hat{B}_1(\alpha_\delta,\beta_\delta,\gamma) & \hat{B}_2(\alpha_\delta,\beta_\delta,\gamma) \\ \hat{C}_1(\alpha_\delta,\beta_\delta,\gamma) & \hat{D}_{11}(\alpha_\delta,\beta_\delta,\gamma) & \hat{D}_{12}(\alpha_\delta,\beta_\delta,\gamma) \end{bmatrix}, \end{aligned} \tag{17}$$

where the relationship between α_δ, β_δ, and γ, and Θ can be found in Eq. (14) and $[\nabla_a H(0)]$ is the partial derivative of the LFT system $H(\Theta)$ in Eq. (16) with respect to a, which can be calculated as shown by Nagamune and Choi (2010). The state-space representation after

performing the Taylor series expansion is given by

$$\begin{bmatrix} x(k+1) \\ z(k) \end{bmatrix} = \begin{bmatrix} \hat{A}(\alpha_\delta,\beta_\delta,\gamma) & \hat{B}_1(\alpha_\delta,\beta_\delta,\gamma) & \hat{B}_2(\alpha_\delta,\beta_\delta,\gamma) \\ \hat{C}_1(\alpha_\delta,\beta_\delta,\gamma) & \hat{D}_{11}(\alpha_\delta,\beta_\delta,\gamma) & \hat{D}_{12}(\alpha_\delta,\beta_\delta,\gamma) \end{bmatrix} \begin{bmatrix} x(k) \\ \tilde{w}(k) \\ u(k) \end{bmatrix}. \tag{18}$$

3.4. An augmented LPV system for synthesis

To create an appropriate measurement for gain-scheduling control, the LPV system $\hat{H}(\Theta)$ must be augmented with the low-pass filter $L(q)$ and the integrator $I(q)$. After augmenting the affine LPV system with the low pass filter and the integrator, the augmented state-space representation is given by

$$\begin{bmatrix} x_{AUG}(k+1) \\ z(k) \\ e(k) \end{bmatrix} = \begin{bmatrix} \tilde{A}(\alpha_\delta,\beta_\delta,\gamma) & \tilde{B}_1(\alpha_\delta,\beta_\delta,\gamma) & \tilde{B}_2(\alpha_\delta,\beta_\delta,\gamma) \\ \tilde{C}_1(\alpha_\delta,\beta_\delta,\gamma) & \tilde{D}_{11}(\alpha_\delta,\beta_\delta,\gamma) & \tilde{D}_{12}(\alpha_\delta,\beta_\delta,\gamma) \\ \tilde{C}_2 & 0 & 0 \end{bmatrix} \begin{bmatrix} x_{AUG}(k) \\ \tilde{w}(k) \\ u(k) \end{bmatrix}, \tag{19}$$

where the augmented states are given by $x_{AUG}(k) = [x(k)^\mathsf{T}\ x_L(k)\ x_I(k)]^\mathsf{T} \in \mathbb{R}^{n_{AUG}}$ with $n_{AUG}=n+2$, and the measurement for control is given by $e(k) = \begin{bmatrix} e_P(k)\ e_I(k) \end{bmatrix}^\mathsf{T} \in \mathbb{R}^q$ with $q=2$. The state-space matrices are given by

$$\tilde{A}(\alpha_\delta,\beta_\delta,\gamma) = \begin{bmatrix} \hat{A}(\alpha_\delta,\beta_\delta,\gamma) & 0 & 0 \\ B_L\hat{C}_1(\alpha_\delta,\beta_\delta,\gamma) & A_L & 0 \\ 0 & C_L & 1 \end{bmatrix},$$

$$\tilde{B}_1(\alpha_\delta,\beta_\delta,\gamma) = \begin{bmatrix} \hat{B}_1(\alpha_\delta,\beta_\delta,\gamma) \\ B_L\hat{D}_{11}(\alpha_\delta,\beta_\delta,\gamma) \\ 0 \end{bmatrix},$$

$$\tilde{B}_2(\alpha_\delta,\beta_\delta,\gamma) = \begin{bmatrix} \hat{B}_2(\alpha_\delta,\beta_\delta,\gamma) \\ B_L\hat{D}_{12}(\alpha_\delta,\beta_\delta,\gamma) \\ 0 \end{bmatrix},$$

$$\tilde{C}_1(\alpha_\delta,\beta_\delta,\gamma) = [\hat{C}_1(\alpha_\delta,\beta_\delta,\gamma)\ \ 0\ \ 0],$$

$$\tilde{C}_2 = \begin{bmatrix} 0 & C_L & 0 \\ 0 & 0 & 1 \end{bmatrix},$$

and $\tilde{D}_{11}(\alpha_\delta,\beta_\delta,\gamma) = \hat{D}_{11}(\alpha_\delta,\beta_\delta,\gamma)$, $\tilde{D}_{12}(\alpha_\delta,\beta_\delta,\gamma) = \hat{D}_{12}(\alpha_\delta,\beta_\delta,\gamma)$. The matrices (A_L, B_L, C_L) represent the state-space matrices of the low-pass filter $L(q)$.

3.5. A gain-scheduling control synthesis problem

Having augmented all components for the controller synthesis, we need to synthesize the $\mathcal{H}_\infty$ gain-scheduling controller $K(\Theta)$. The ℓ_2 gain of the LPV system in Eq. (19) with a gain-scheduling feedback controller is defined as

$$\max_{\Theta\in\mathbf{\Theta},\ \|\tilde{w}\|_{\ell_2}\neq 0} \frac{\|z\|_{\ell_2}}{\|\tilde{w}\|_{\ell_2}}. \tag{20}$$

Now we formally state the gain-scheduling control design problem.

Problem. The goal is to design a static gain-scheduling control $u(k) = K(\Theta)e(k)$ that stabilizes the closed-loop system and minimizes the worst-case ℓ_2 gain ($\mathcal{H}_\infty$ norm) of the closed-loop LPV system in Eq. (20) for any trajectories of $\Theta(k) \in \mathbf{\Theta}$.

The gain-scheduling method provided by Caigny et al. (2008) guarantees an $\mathcal{H}_\infty$ cost such that for an exogenous input $\tilde{w}$, the performance output z satisfies

$$\|z\|_{\ell_2} < \eta\|\tilde{w}\|_{\ell_2},$$

for any trajectories of $\Theta(k) \in \mathbf{\Theta}$. This method was derived for discrete-time polytopic time-varying systems. Therefore, in the next section, we will transform our augmented system into a polytopic time-varying system to synthesize the controller.

3.6. Controller synthesis for polytopic linear time-varying system

The augmented state-space representation $(\tilde{A}(\alpha_\delta,\beta_\delta,\gamma),\ \tilde{B}_1(\alpha_\delta,\beta_\delta,\gamma),\ \ldots)$ in Eq. (19) can be converted into a discrete-time polytopic time-varying system $(\overline{A}[\lambda(k)],\ \overline{B}_1[\lambda(k)],\ \ldots)$ using the state-space matrices at vertices $\{\mathcal{V}_i\}$ of the parameter space polytope displayed in Fig. 7. Any system inside of the convex parameter set is represented by a convex combination of the vertex systems as weighted by the vector $\lambda(k)$ of barycentric coordinates. Barycentric coordinates are used to specify the location of a point as the center of mass, or barycenter, of masses placed at the vertices of a simplex. Warren, Schaefer, Hirani, and Desbrun (2007) provide a formula, which is covered in Appendix A.4, for computing the barycentric coordinates for any convex polytope. The discrete-time polytopic linear time-varying system is given by

$$\begin{bmatrix} x(k+1) \\ z(k) \\ e(k) \end{bmatrix} = \begin{bmatrix} \overline{A}[\lambda(k)] & \overline{B}_1[\lambda(k)] & \overline{B}_2[\lambda(k)] \\ \overline{C}_1[\lambda(k)] & \overline{D}_{11}[\lambda(k)] & \overline{D}_{12}[\lambda(k)] \\ \overline{C}_2 & 0 & 0 \end{bmatrix} \begin{bmatrix} x(k) \\ w(k) \\ u(k) \end{bmatrix},$$

$$e(k) = [e_P(k)\ \ e_I(k)]^\mathsf{T}, \tag{21}$$

where, for all $k \in \mathbb{Z}_{\geq 0}$, $\lambda(k)$ is the vector of time-varying barycentric coordinates that belong to the unit simplex

$$\Lambda_N = \left\{ \zeta \in \mathbb{R}^N : \sum_{i=1}^{N} \zeta_i = 1, \zeta_i \geq 0, i = 1,\ldots,N \right\},$$

where N is the number of vertices of the polytope. A way to compute the barycentric coordinate vector $\lambda(k)$ for a given $\alpha_\delta(k)$, $\beta_\delta(k)$, and $\gamma(k)$ is provided in Appendix A.4. For all $k \in \mathbb{Z}_{\geq 0}$, the rate of variation of the weights

$$\Delta\lambda_i(k) = \lambda_i(k+1) - \lambda_i(k), \quad i = 1,\ldots,N$$

is limited by the calculated bound b such that

$$b\lambda_i(k) \leq \Delta\lambda_i(k) \leq b(1-\lambda_i(k)), \quad i = 1,\ldots,N, \tag{22}$$

where $b \in [0,1]$.

The system matrices $\overline{A}[\lambda(k)] \in \mathbb{R}^{n_{AUG}\times n_{AUG}}$, $\overline{B}_1[\lambda(k)] \in \mathbb{R}^{n_{AUG}\times r}$, $\overline{B}_2[\lambda(k)] \in \mathbb{R}^{n_{AUG}\times m}$, $\overline{C}_1[\lambda(k)] \in \mathbb{R}^{p\times n_{AUG}}$, $\overline{D}_{11}[\lambda(k)] \in \mathbb{R}^{p\times r}$, $\overline{D}_{12}[\lambda(k)] \in \mathbb{R}^{p\times m}$ belong to the polytope

$$\mathcal{D} = \{(\overline{A},\overline{B}_1,\overline{B}_2,\overline{C}_1,\overline{D}_{11},\overline{D}_{12})(\lambda(k)) : (\overline{A},\overline{B}_1,\overline{B}_2,\overline{C}_1,\overline{D}_{11},\overline{D}_{12})(\lambda(k)) = \sum_{i=1}^{N} \lambda_i(k)(\overline{A},\overline{B}_1,\overline{B}_2,\overline{C}_1,\overline{D}_{11},\overline{D}_{12})_i, \lambda(k) \in \Lambda_N\}.$$

The system matrices at any time k are the weighted summation of vertex system matrices $\{\mathcal{V}_i\}$ weighted by their barycentric

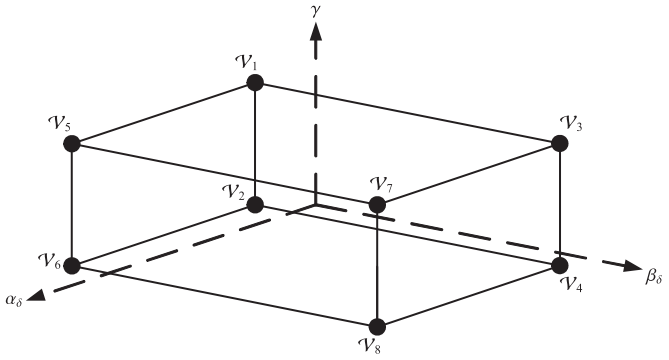

Fig. 7. Parameter space polytope.

coordinates $\lambda_i(k)$, i.e.,

$$\overline{A}(k) = \sum_{i=1}^{N} \lambda_i(k)\overline{A}(\mathcal{V}_i), \quad i = 1, \ldots, N.$$

The same computation holds for $\overline{B}_1$, $\overline{B}_2$, $\overline{C}_1$, $\overline{D}_{11}$, and $\overline{D}_{12}$ as well.

A finite set of LMIs in Caigny et al. (2008) can be used to design the gain-scheduling controller. Due to Theorem 3 of Caigny et al. (2008), if there exists matrices $G_{i,1} \in \mathbb{R}^{q\times q}$, $G_{i,2} \in \mathbb{R}^{(n_{AUG}-q)\times q}$, $G_{i,3} \in \mathbb{R}^{(n_{AUG}-q)\times(n_{AUG}-q)}$, $Z_{i,1} \in \mathbb{R}^{m\times q}$ and symmetric matrices $P_i \in \mathbb{R}^{n_{AUG}\times n_{AUG}}$ such that the LMI conditions in Eqs. (24) and (25) are satisfied, the gain-scheduling static feedback control is then obtained as

$$K(\lambda(k)) = \hat{Z}(\lambda(k))\hat{G}(\lambda(k))^{-1}, \tag{23}$$

where

$$\hat{Z}(\lambda(k)) = \sum_{i=1}^{N} \lambda_i(k)Z_{i,1} \quad \text{and} \quad \hat{G}(\lambda(k)) = \sum_{i=1}^{N} \lambda_i(k)G_{i,1}.$$

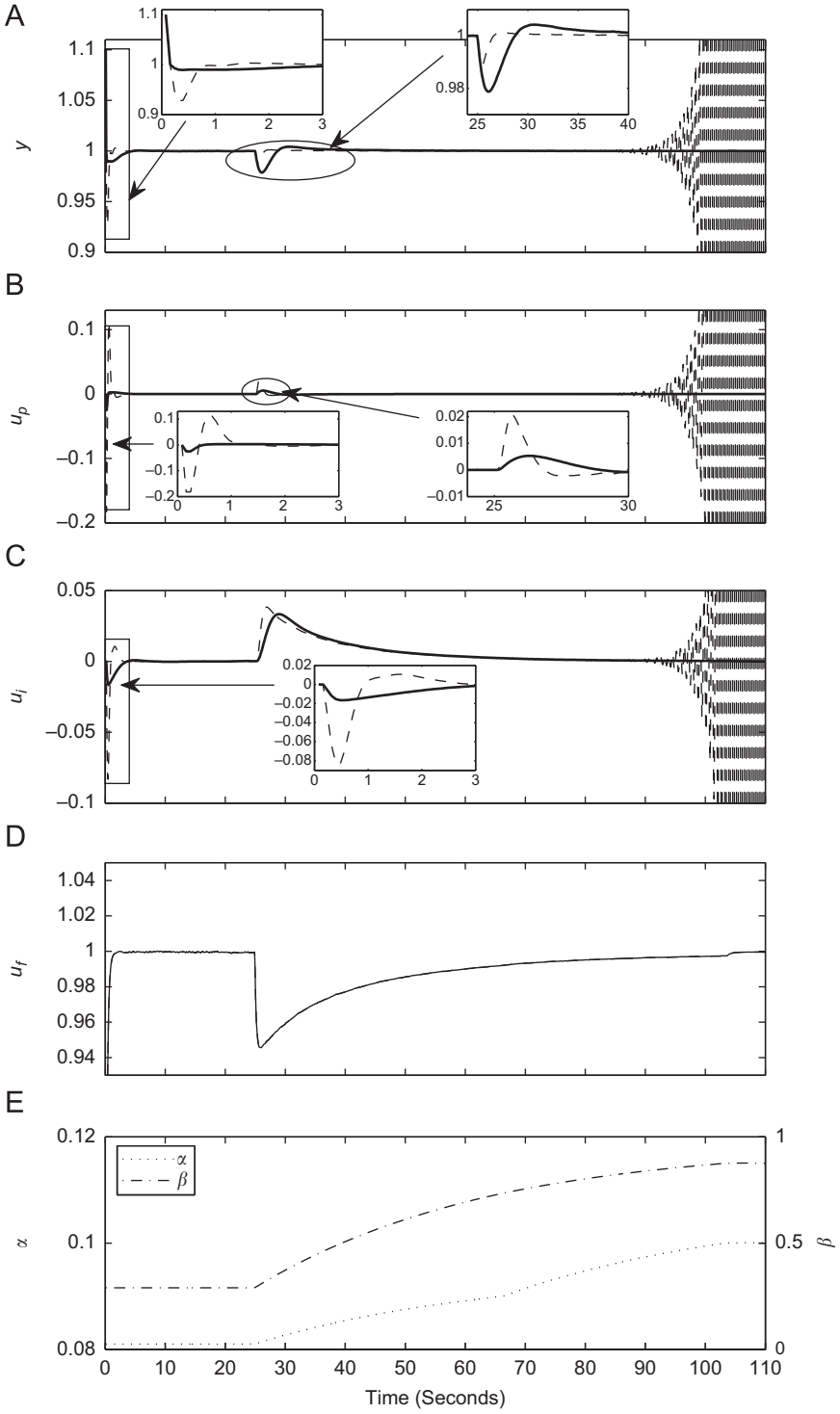

Fig. 8. Case 1 engine cold start: in plots A, B, C, and D the equivalence ratio $y(k)$, proportional control $u_p(k)$, integral control $u_i(k)$, and the feed-forward control are compared for the gain-scheduling feedback controller (solid line) and the fixed $\mathcal{H}_\infty$ controller (dashed line). The time-varying parameters α (dotted line, left axis) and β (dash-dot line, right axis) are displayed in plot E.

This control is proved to stabilize affine parameter-dependent systems such as (21) with a guaranteed $\mathcal{H}_\infty$ performance bounded by η for all $\lambda \in \Lambda_N$ and $\Delta\lambda$ that satisfies (22).

The LMIs in Eqs. (24) and (25) are solved by programming them into MATLAB using the LMI lab (Gahinet, Nemirovski, Laub, & Chilali, 1995) in the Robust Control toolbox. The matrices $G_{i,1}$, $G_{i,2}$, $G_{i,3}$, $Z_{i,1}$, P_i, and the $\mathcal{H}_\infty$ cost η are programmed in MATLAB as free matrix variables for the LMI optimization to choose. Since all LMIs are constructed using symmetric matrices, $\star$ represents entries which follow from symmetry. During the solution process, the $\mathcal{H}_\infty$ cost η is minimized until the optimal solution is obtained by using the following LMIs:

$$\begin{bmatrix} (1-b)P_i + bP_\ell & \star & \star & \star \\ G_i^T\overline{A}_i^T + Z_i^T\overline{B}_{2,i}^T & G_i + G_i^T - P_i & \star & \star \\ \overline{B}_{1,i}^T & 0 & \eta I & \star \\ 0 & \overline{C}_{1,i}G_i + \overline{D}_{12,i}Z_i & \overline{D}_{11,i} & \eta I \end{bmatrix} \succ 0 \tag{24}$$

hold for $i = 1,\ldots,N$ and $\ell = 1,\ldots,N$ and

$$\begin{bmatrix} (1-b)P_i + (1-b)P_j + 2bP_\ell & \star & \star & \star \\ G_j^T\overline{A}_i^T + G_i^T\overline{A}_j^T + Z_j^T\overline{B}_{2,i}^T + Z_i^T\overline{B}_{2,j}^T & G_i + G_i^T + G_j + G_j^T - P_i - P_j & \star & \star \\ \overline{B}_{1,i}^T + \overline{B}_{1,j}^T & 0 & 2\eta I & \star \\ 0 & \overline{C}_{1,i}G_j + \overline{C}_{1,j}G_i + \overline{D}_{12,i}Z_j + \overline{D}_{12,j}Z_i & \overline{D}_{11,i} + \overline{D}_{11,j} & 2\eta I \end{bmatrix} \succ 0 \tag{25}$$

hold for $\ell = 1,\ldots,N$, $i = 1,\ldots,N-1$, and $j = i+1,\ldots,N$, with

$$G_i = \begin{bmatrix} G_{i,1} & 0 \\ G_{i,2} & G_{i,3} \end{bmatrix} \quad \text{and} \quad Z_i = [Z_{i,1} \;\; 0].$$

4. Simulation results

To validate the effectiveness of the proposed gain-scheduling controller, simulations are shown using the original plant in Eq. (13) for the following cases: engine cold start, load change, and engine speed change.

The necessity of a gain-scheduled controller is demonstrated by comparing its performance with that of a fixed gain $\mathcal{H}_\infty$ controller for the nominal parameters. The fixed gain $\mathcal{H}_\infty$ control synthesis procedure is reviewed in Appendix A.5.

In each simulation, the time-varying parameters α and β are corrupted by low-pass filtered white noise of up to 10% their nominal values to represent the slowly drifting offset that might occur in practical situations. To see transient responses, the initial conditions of the plant for Case 1 were chosen such that a little extra fuel is injected at first, giving a slightly higher equivalence ratio than 1. The initial conditions in Cases 2 and 3 were set such that the plant would start with an equivalence ratio of 1. For the following simulation cases, the extracted profiles of time-varying parameters from engine dynamometer tests were used.

4.1. Case 1: engine cold start

We simulate an engine operation when it was started at freezing temperatures (0 °C) and heated to its normal operation temperature of approximately 100 °C within about 2 min at an engine speed of 1500 rpm. The purpose of this simulation is to emulate the cold start of an internal combustion engine when the engine is operated at high idle speed during the warm-up. Note that during the engine warm-up process the fuel vapor is much less at low temperature than that at high temperature. Therefore, this leads to quite different wall-wetting dynamics. The wall-wetting dynamics coefficients α and β defined in Eq. (3) were obtained from actual engine test data and they are functions of engine cylinder head temperature, speed and load. Since speed and load are fixed in this simulation, both α and β are functions of engine temperature and their values are shown in Fig. 8E. Notice that the transient response at 25 s in Fig. 8 is due to the change in the wall-wetting parameters as shown in Fig. 8E. When the engine has been warming up for about 90 s, the closed-loop system with the fixed $\mathcal{H}_\infty$ controller becomes unstable, while the LPV controller remains stable. Thus, in Fig. 8A, one can readily see the LPV controller's advantage of guaranteed stability as the parameters vary with time.

4.2. Case 2: load change

In this case we simulate an engine dynamometer experiment for an engine operated at a temperature of 80 °C with an engine speed of 1500 rpm. After the engine is stably operated at this condition with a 32% throttle, the load is increased by a step throttle position from 32% to 46%. Note that in the dynamometer test, the engine speed was maintained by dynamometer by increasing the load torque. This is similar to the driving condition that a step throttle is applied to maintain the vehicle speed when the vehicle is driven up a hill. Note that the step increment of throttle position produces a

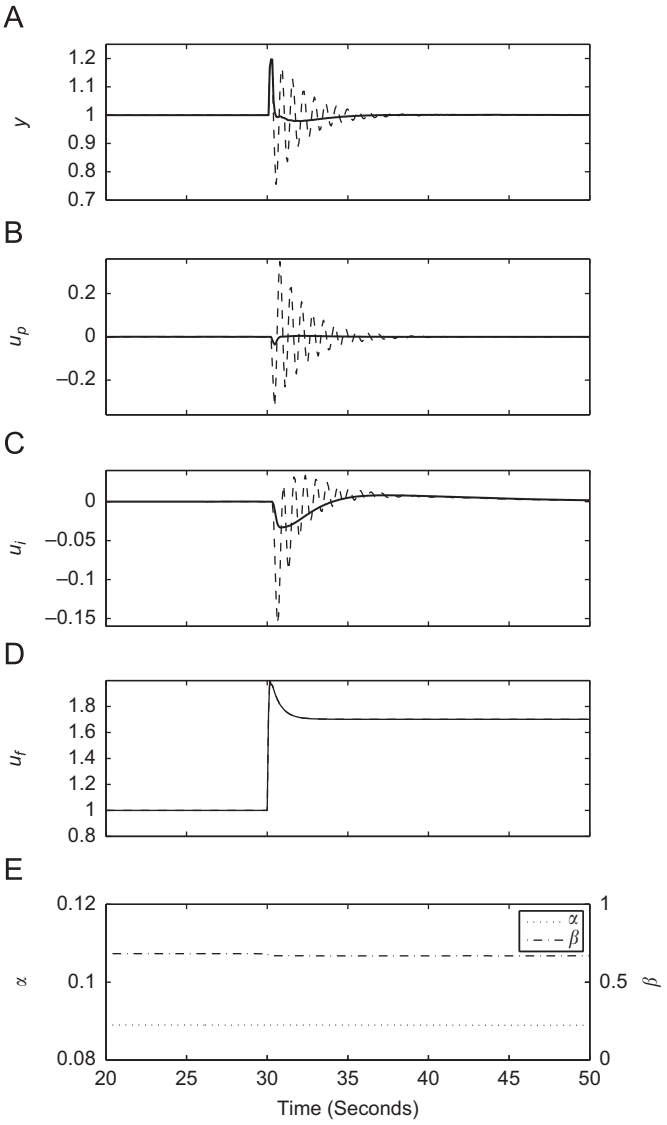

Fig. 9. Case 2 load change: in plots A, B, C, and D the equivalence ratio $y(k)$, proportional control $u_p(k)$, integral control $u_i(k)$, and the feed-forward control are compared for the gain-scheduling feedback controller (solid line) and the fixed $\mathcal{H}_\infty$ controller (dashed line). The time-varying parameters α (dotted line, left axis) and β (dash-dot line, right axis) are displayed in plot E.

slight change in the wall-wetting parameter β as shown in Fig. 9E. But in Fig. 9, one can find the benefit of guaranteed performance of the gain-scheduling controller over the time-varying parameters. Note that the step throttle occurred at the 30th second results in a momentary spike in the equivalence ratio due to the step air mass flow; but it is quickly pulled back into its target level by the gain-scheduled controller, while the fixed $\mathcal{H}_\infty$ controller takes much longer time with a lot of oscillations and uses more control effort.

4.3. Case 3: engine speed change

In this simulation, an engine was operated in a dynamometer with its cylinder head temperature at 80 °C. To demonstrate the capability for the gain-scheduling controller to handle fast engine speed variations, smoothed step commands were applied to the engine dynamometer to manipulate the engine speeds shown in Fig. 10F. The resulting engine wall-wetting dynamic parameters, shown in Fig. 10E, were used in the simulation. In Fig. 10A, one can see that both controllers, gain-scheduling and fixed $\mathcal{H}_\infty$, regulate the engine equivalence ratio to its target value of one within 5% error except at 25th second when the engine speed was increased abruptly from 1000 to 4500 rpm. In this case, the engine equivalence ratio response converges to its target value smoothly for the gain-scheduling controller but with a lot of oscillations for the fixed $\mathcal{H}_\infty$ controller. This situation is similar to a transmission gear shifting where a rapid engine speed change may occur. Again, one

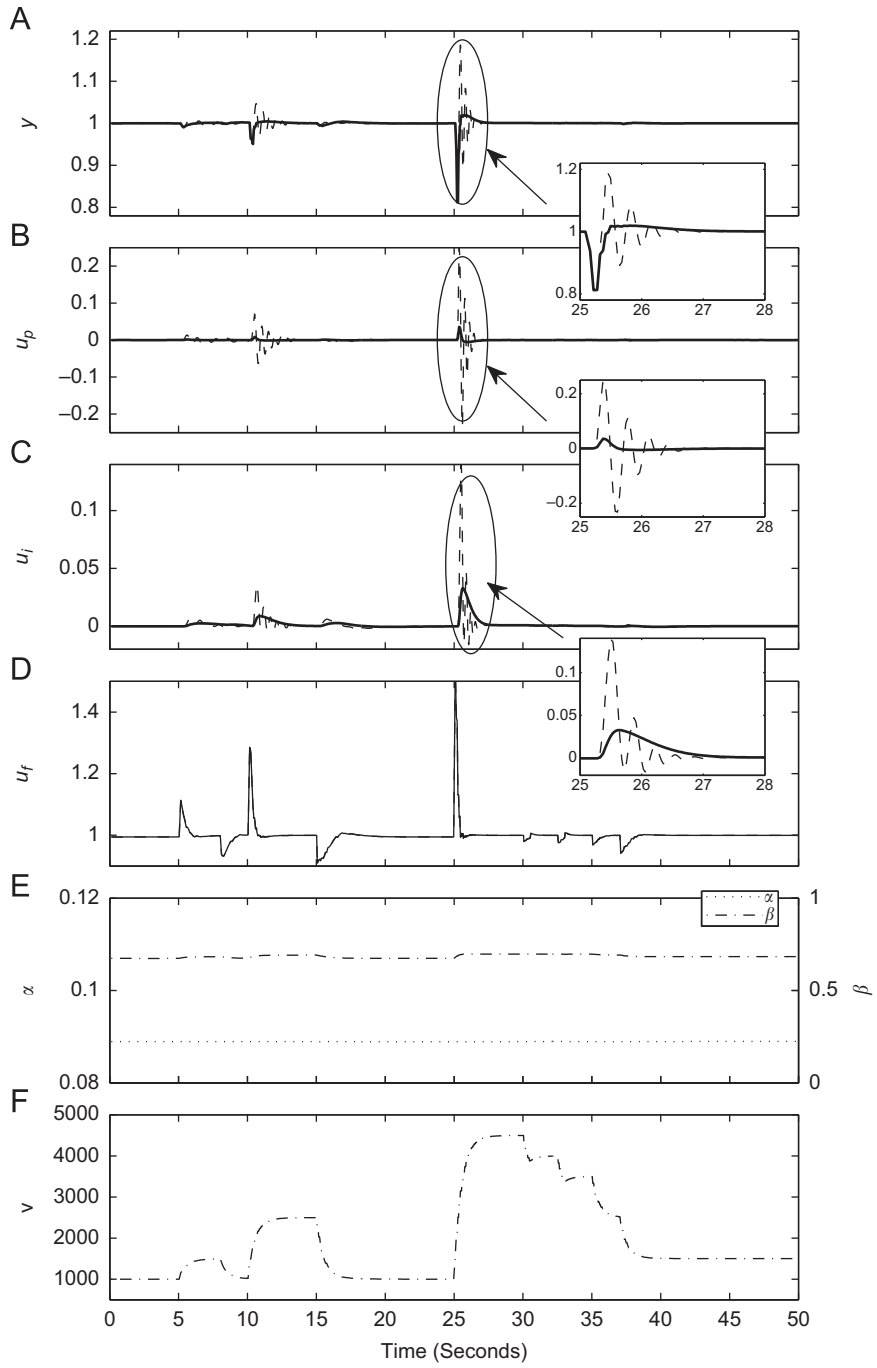

Fig. 10. Case 3 engine speed change: in plots A, B, C, and D the equivalence ratio $y(k)$, proportional control $u_p(k)$, integral control $u_i(k)$, and the feed-forward control are compared for the gain-scheduling feedback controller (solid line) and the fixed $\mathcal{H}_\infty$ controller (dashed line). The wall-wetting parameters α (dotted line, left axis) and β (dash-dot line, right axis) are displayed in plot E. The engine speed v is displayed in plot F.

can see the advantage of guaranteed performance over the time-varying parameters as the gain-scheduled controller regulates the equivalence ratio back into safe limits quicker and with less overshoot than the fixed $\mathcal{H}_\infty$ controller.

5. Summary

In this paper, a systematic process for developing gain-scheduling PI controllers for discrete-time LPV systems is presented. First, a control oriented LPV model is developed using the dynamics of a port-fuel-injection process. Then the LPV model obtained is investigated and found to contain parameter variation that is not affine. Due to limitations in current LPV control schemes for discrete-time systems discussed in Section 3.3, a first-order Taylor series approximation is performed on the LPV system $H(\Theta)$ in (16) to obtain an approximated LPV system $\hat{H}(\Theta)$ in (17) with only affine parameter variation. The measurement for control is generated by augmenting the approximated LPV system with a low-pass filter and an integrator. The augmented, approximated LPV system is then converted to a polytopic LPV system so that the synthesis method given by Caigny et al. (2008) can be utilized. To validate the gain-scheduling controller found with the finally obtained LPV system $\hat{H}(\Theta)$, simulations are performed using the original LPV system $H(\Theta)$. From the simulation results, it is clear that although the approximated LPV system $\hat{H}(\Theta)$ is used to design the gain-scheduling controller it still performs very well when applied to the original LPV system $H(\Theta)$.

Appendix A

A.1. Linear fractional transformation

For completeness, we will now give the definition of a linear fractional transformation (LFT). Linear fractional transformations are used to efficiently formulate the interconnection of multi-input multi-output sub-systems with multiple sources, such as uncertainties, noises, disturbances, and varying parameters. As given by Zhou et al. (1996), the possibly complex coefficient matrix M is partitioned as

$$M=\begin{bmatrix} M_{11} & M_{12} \\ M_{21} & M_{22} \end{bmatrix} \in \mathbb{C}^{(p_1+p_2)\times(q_1+q_2)} \tag{26}$$

with $\Delta_\ell \in \mathbb{C}^{q_2\times p_2}$ and $\Delta_u \in \mathbb{C}^{q_1\times p_1}$. A lower LFT is given with respect to Δ_ℓ as

$$\mathcal{F}_\ell(M,\Delta_\ell)=M_{11}+M_{12}\Delta_\ell(I-M_{22}\Delta_\ell)^{-1}M_{21}. \tag{27}$$

An upper LFT is given with respect to Δ_u by

$$\mathcal{F}_u(M,\Delta_u)=M_{22}+M_{21}\Delta_u(I-M_{11}\Delta_u)^{-1}M_{12}. \tag{28}$$

From the diagrams in Fig. 11, the reason behind the terminology of lower and upper LFTs should be clear. The set of equations representing the lower LFT diagram in Fig. 11A are given by

$$\begin{bmatrix} z_1 \\ y_1 \end{bmatrix}=\begin{bmatrix} M_{11} & M_{12} \\ M_{21} & M_{22} \end{bmatrix}\begin{bmatrix} w_1 \\ u_1 \end{bmatrix},$$

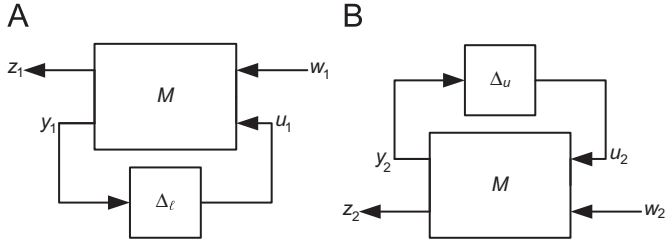

Fig. 11. (A) Diagram of a lower LFT. (B) Diagram of an upper LFT.

$$u_1=\Delta_\ell y_1, \tag{29}$$

and the equations representing Fig. 11B are given by

$$\begin{bmatrix} y_2 \\ z_2 \end{bmatrix}=\begin{bmatrix} M_{11} & M_{12} \\ M_{21} & M_{22} \end{bmatrix}\begin{bmatrix} u_2 \\ w_2 \end{bmatrix},$$

$$u_2=\Delta_u y_2. \tag{30}$$

The partitioning of M depends on the interconnections with the isolated parameter Δ_ℓ or Δ_u and can be determined using the MATLAB function "sysic" (Balas, Doyle, Glover, Packard, & Smith, 2001).

A.2. Oxygen sensor modeling details

To capture this parameter variation, the components of the transfer function diagram in Fig. 2 are now covered in detail. The transport delay used here is $T_D=80/v$. To solve for $A_{O_2 d}$, first A_{O_2} is multiplied by t_s

$$A_{O_2}t_s=\begin{bmatrix} -\frac{v}{80} & \frac{v}{80} \\ 0 & -\frac{1}{T_{O_2}} \end{bmatrix}\frac{120}{v}=\begin{bmatrix} -\frac{3}{2} & \frac{3}{2} \\ 0 & -\frac{120}{T_{O_2}v} \end{bmatrix}. \tag{31}$$

Next, the matrix exponent of $A_{O_2}t_s$ is computed, which gives

$$A_{O_2 d}=\begin{bmatrix} \exp(-\frac{3}{2}) & p_1(v) \\ 0 & p_2(v) \end{bmatrix}, \tag{32}$$

where

$$p_1(v)=\frac{-\frac{3}{2}\left(\exp(-\frac{3}{2})-\exp\left(-\frac{120}{T_{O_2}v}\right)\right)}{-\frac{120}{T_{O_2}v}+\frac{3}{2}}, \tag{33a}$$

$$p_2(v)=\exp\left(-\frac{120}{T_{O_2}v}\right). \tag{33b}$$

To represent the parameter variation in $A_{O_2 d}$, a fourth-order Taylor series approximation of $p_1(v)$ and $p_2(v)$ is used. To ensure that the coefficients of the Taylor series approximations of $p_1(v)$ and $p_2(v)$ are numerically stable with respect to the condition number (Trefethen & Bau, 1997), $1/v$ is normalized. The normalization used is given in Eq. (7) in Section 2.3, but is reproduced here

$$\gamma=\frac{\frac{1}{v}-\frac{1}{v_0}}{\frac{1}{v}+\frac{1}{v_0}} \quad \text{where} \quad \frac{1}{v_0}=\frac{\frac{1}{\bar{v}}+\frac{1}{\underline{v}}}{2}.$$

Solving Eq. (7) for $1/v$, and substituting into Eqs. (33a) and (33b), $p_1(\gamma)$ and $p_2(\gamma)$ are found to be

$$p_1(\gamma)=\frac{-\frac{3}{2}\left(\exp(-\frac{3}{2})-\exp\left(-\frac{120}{T_{O_2}v_0}\left(\frac{1+\gamma}{1-\gamma}\right)\right)\right)}{-\frac{120}{T_{O_2}v_0}\left(\frac{1+\gamma}{1-\gamma}\right)+\frac{3}{2}}, \tag{34a}$$

$$p_2(\gamma)=\exp\left(-\frac{120}{T_{O_2}v_0}\left(\frac{1+\gamma}{1-\gamma}\right)\right). \tag{34b}$$

Finally, $A_{O_2 d}$ is represented with the following lower LFT:

$$A_{O_2 d}=\mathcal{F}_\ell(M_{A_{O_2 d}},\gamma I_n), \tag{35}$$

where

$$M_{A_{O_2 d}}=\left[\begin{array}{cc|ccc} \exp\left(-\frac{3}{2}\right) & a_0 & a_1 & \cdots & a_n \\ 0 & b_0 & b_1 & \cdots & b_n \\ \hline 0 & 1 & \multicolumn{3}{c}{0_{1\times n}} \\ \multicolumn{2}{c|}{0_{(n-1)\times 2}} & \multicolumn{3}{c}{I_{(n-1)\times(n-1)}\quad 0_{(n-1)\times 1}} \end{array}\right] \tag{36}$$

and

$$a_n = \frac{1}{n!}\frac{d^n p_1(0)}{d\gamma^n},$$

$$b_n = \frac{1}{n!}\frac{d^n p_2(0)}{d\gamma^n}.$$

From Eq. (6), recall that $B_{O_2 d} = A_{O_2}^{-1}(A_{O_2 d} - I)B_{O_2}$. Since $A_{O_2 d}$ is already found, $A_{O_2}^{-1}$ is now computed.

$$A_{O_2}^{-1} = T_D T_{O_2} \begin{bmatrix} -\frac{1}{T_{O_2}} & -\frac{1}{T_D} \\ 0 & -\frac{1}{T_D} \end{bmatrix} = \begin{bmatrix} -T_D & -T_{O_2} \\ 0 & -T_{O_2} \end{bmatrix} = \begin{bmatrix} -\frac{80}{v} & -T_{O_2} \\ 0 & -T_{O_2} \end{bmatrix}. \quad (37)$$

Thus, $A_{O_2}^{-1}$ can be represented with the following lower LFT:

$$A_{O_2}^{-1} = \mathcal{F}_\ell\left(M_{A_{O_2}^{-1}}, \frac{1}{v}\right), \quad (38)$$

where

$$M_{A_{O_2}^{-1}} = \left[\begin{array}{cc:c} 0 & -T_{O_2} & -80 \\ 0 & -T_{O_2} & 0 \\ \hdashline 1 & 0 & 0 \end{array}\right]. \quad (39)$$

To normalize $1/v$ to γ, the following upper LFT is used:

$$\frac{1}{v} = \mathcal{F}_u(M_\gamma, \gamma), \quad \text{where} \quad M_\gamma = \left[\begin{array}{c:c} \frac{1}{2} & \frac{1}{2} \\ \hdashline \frac{1}{v_0} & \frac{1}{v_0} \end{array}\right]. \quad (40)$$

A.3. System matrices

The state-space matrices for the LPV system in (13) have been found to be

$$A = \begin{bmatrix} 0.91 & 0 & 0.0369 & 0 & 0 & 0 & 0 & 0 \\ 0.2617 & 0 & 0.1544 & 0 & 0 & 1.4352 & 0 & 0 \\ 0 & 0 & 0.8475 & 0 & 0 & 0 & 0 & 0 \\ 0 & 1.4506 & 0 & 0.2231 & 0.3972 & 0 & 0 & 0 \\ 0 & 2.6311 & 0 & 0 & 0.3114 & 0 & 0 & 0 \\ 0 & 0 & 0 & 0 & 0 & 0.9986 & 0 & 0 \\ 0 & 0 & 0 & 0 & 0 & 0 & 1.9972 & -0.9985 \\ 0 & 0 & 0 & 0 & 0 & 0 & 0.9987 & 0 \end{bmatrix} \in \mathbb{R}^{8\times 8},$$

$$B_0 = \begin{bmatrix} -0.09 & 0.0625 & 0 & 0 & 1 & 0 & 0 & 0 & 0 & 0 & 0 & 0 & 0 & 0 \\ 0.2617 & 0.2617 & 0 & 0 & 0 & 0 & 0 & 0 & 0 & 0 & 0 & 0 & 0 & 0 \\ 0 & -0.2585 & 1.6949 & 1.6949 & 0 & 0 & 0 & 0 & 0 & 0 & 0 & 0 & 0 & 0 \\ 0 & 0 & 0 & 0 & 0 & 0.0664 & -0.0027 & -0.0214 & -0.0179 & -0.0933 & -0.4891 & -0.0984 & 0.0608 & 0.0975 \\ 0 & 0 & 0 & 0 & 0 & 0.0436 & -0.0073 & -0.0186 & -0.0134 & 0 & -0.7266 & 0.1211 & 0.3095 & 0.2231 \\ 0 & 0 & 0 & 0 & 0 & 0 & 0 & 0 & 0 & 0 & 0 & 0 & 0 & 0 \\ 0 & 0 & 0 & 0 & 0 & 0 & 0 & 0 & 0 & 0 & 0 & 0 & 0 & 0 \\ 0 & 0 & 0 & 0 & 0 & 0 & 0 & 0 & 0 & 0 & 0 & 0 & 0 & 0 \end{bmatrix} \in \mathbb{R}^{8\times 14},$$

$$B_1 = \begin{bmatrix} 0 & 0 & 0.0043 \\ 0 & 0 & 0.0179 \\ 0 & 0 & -0.0073 \\ 0 & 0 & 0 \\ 0 & 0 & 0 \\ 0.3756 & 0 & 0 \\ 0 & 0.0266 & 0 \\ 0 & 0 & 0 \end{bmatrix} \in \mathbb{R}^{8\times 3}, \quad B_2 = \begin{bmatrix} 0.0369 \\ 0.1544 \\ 0 \\ 0 \\ 0 \\ 0 \\ 0 \\ 0 \end{bmatrix} \in \mathbb{R}^{8\times 1},$$

$$C_0 = \begin{bmatrix} 0 & 0 & 1 & 0 & 0 & 0 & 0 & 0 \\ 0 & 0 & 0 & 0 & 0 & 0 & 0 & 0 \\ 0 & 0 & 0.1525 & 0 & 0 & 0 & 0 & 0 \\ 0 & 0 & -1 & 0 & 0 & 0 & 0 & 0 \\ -1 & 0 & 0.41 & 0 & 0 & 0 & 0 & 0 \\ 0 & 63.6832 & 0 & 0 & 0 & 0 & 0 & 0 \\ 0 & 0 & 0 & 0 & 0 & 0 & 0 & 0 \\ 0 & 0 & 0 & 0 & 0 & 0 & 0 & 0 \\ 0 & 0 & 0 & 0 & 0 & 0 & 0 & 0 \\ 0 & 25.2968 & 0 & 0 & 0 & 0 & 0 & 0 \\ 0 & 0 & 0 & 0 & 1 & 0 & 0 & 0 \\ 0 & 0 & 0 & 0 & 0 & 0 & 0 & 0 \\ 0 & 0 & 0 & 0 & 0 & 0 & 0 & 0 \\ 0 & 0 & 0 & 0 & 0 & 0 & 0 & 0 \end{bmatrix} \in \mathbb{R}^{14\times 8}, \quad C_1 = [0\ 0\ 0\ -1\ 0\ 0\ 0.015\ 0.015] \in \mathbb{R}^{1\times 8},$$

$$D_{00}=\begin{bmatrix}
0 & 1.6949 & 0 & 0 & 0 & 0 & 0 & 0 & 0 & 0 & 0 & 0 & 0 & 0 \\
0 & -1.6949 & 0 & 0 & 0 & 0 & 0 & 0 & 0 & 0 & 0 & 0 & 0 & 0 \\
0 & 0.2585 & -1.6949 & -1.6949 & 0 & 0 & 0 & 0 & 0 & 0 & 0 & 0 & 0 & 0 \\
0 & -1.6949 & 0 & 0 & 0 & 0 & 0 & 0 & 0 & 0 & 0 & 0 & 0 & 0 \\
-1 & 0.6949 & 0 & 0 & 0 & 0 & 0 & 0 & 0 & 0 & 0 & 0 & 0 & 0 \\
0 & 0 & 0 & 0 & 0 & 0 & 0 & 0 & 0 & 0 & 0 & 0 & 0 & 0 \\
0 & 0 & 0 & 0 & 0 & 0 & 1 & 0 & 0 & 0 & 0 & 0 & 0 & 0 \\
0 & 0 & 0 & 0 & 0 & 0 & 0 & 1 & 0 & 0 & 0 & 0 & 0 & 0 \\
0 & 0 & 0 & 0 & 0 & 0 & 0 & 0 & 1 & 0 & 0 & 0 & 0 & 0 \\
0 & 0 & 0 & 0 & 0 & 0 & -0.4891 & -0.0984 & 0.0608 & 0.0975 & 1 & 0 & 0 & 0 \\
0 & 0 & 0 & 0 & 0 & 0 & 0 & 0 & 0 & 0 & 0 & 0 & 0 & 0 \\
0 & 0 & 0 & 0 & 0 & 0 & 0 & 0 & 0 & 0 & 0 & 1 & 0 & 0 \\
0 & 0 & 0 & 0 & 0 & 0 & 0 & 0 & 0 & 0 & 0 & 0 & 1 & 0 \\
0 & 0 & 0 & 0 & 0 & 0 & 0 & 0 & 0 & 0 & 0 & 0 & 0 & 1
\end{bmatrix}\in\mathbb{R}^{14\times 14},$$

$$D_{01}=\begin{bmatrix}
0 & 0 & 0.1161 & 1 \\
0 & 0 & -0.1161 & 0 \\
0 & 0 & 0.0073 & 0 \\
0 & 0 & -0.0476 & 0 \\
0 & 0 & 0.0476 & 0.41 \\
0 & 0 & 0 & 0 \\
0 & 0 & 0 & 0 \\
0 & 0 & 0 & 0 \\
0 & 0 & 0 & 0 \\
0 & 0 & 0 & 0 \\
0 & 0 & 0 & 0 \\
0 & 0 & 0 & 0 \\
0 & 0 & 0 & 0 \\
0 & 0 & 0 & 0
\end{bmatrix}\in\mathbb{R}^{14\times 3},\quad D_{02}=\begin{bmatrix}
1 \\ 0 \\ 0 \\ 0 \\ 0.41 \\ 0 \\ 0 \\ 0 \\ 0 \\ 0 \\ 0 \\ 0 \\ 0 \\ 0
\end{bmatrix}\in\mathbb{R}^{14\times 1},$$

$$D_{10}=[0\ 0\ 0\ 0\ 0\ 0\ 0\ 0\ 0\ 0\ 0\ 0\ 0\ 0]\in\mathbb{R}^{1\times 14},\quad D_{10}=[0\ 0\ 0]\in\mathbb{R}^{1\times 14},\quad D_{10}=[0]\in\mathbb{R}. \tag{41}$$

A.4. Barycentric coordinates

The parameter variation is contained inside of the convex polytope. The gain-scheduling control used (Caigny et al., 2008) requires that the parameter variation be expressed as a combination of the vertices of this polytope. In order to compute the convex combination coefficients $\{\lambda_i(\Theta)\}$ for a given Θ and vertices $\{\mathcal{V}_i\}$, barycentric coordinates are used. The barycentric coordinate function is defined as

$$\lambda_i(\Theta)=\frac{\Upsilon_i(\Theta)}{\sum_i \Upsilon_i(\Theta)}, \tag{42}$$

where $\Upsilon_i(\Theta)$ is the weight function of vertex i for a point Θ inside of the convex polytope. The weight function is

$$\Upsilon_i(\Theta)=\frac{\mathrm{vol}(\mathcal{V}_i)}{\prod_{j\in\{1,2,3\}}(n_j\cdot(\mathcal{V}_i-\Theta))}, \tag{43}$$

where vol $(\mathcal{V}_i)$ is the volume of the parallelepiped span by the normals to the facets incident on vertex i, i.e., $\mathcal{V}_i$ (Warren et al., 2007). $\{n_j\}$ is the collection of normal vectors to the facets incident on vertex i. The volume of a parallelepiped can be found as

$$\mathrm{vol}(\mathcal{V}_i)=\left|\det\begin{bmatrix}n_1\\ n_2\\ n_3\end{bmatrix}\right|. \tag{44}$$

A.5. Design of LTI feedback controller

The open-loop state-space plant used for designing this controller is the same as the one in Fig. 6, but has the low-pass filter $L(q)$ and the integrator $I(q)$ added without performing any Taylor series expansion. Using the nominal parameters, the closed-loop state-space representation is

$$\begin{aligned}x(k+1)&=A_{CL}(K)x(k)+B_1w(k),\\ z(k)&=C_{CL}(K)x(k)+D_{11}w(k),\end{aligned} \tag{45}$$

where

$$A_{CL}(K)=A+B_2KC_2\quad\text{and}\quad C_{CL}(K)=C_1+D_{12}KC_2.$$

Denoting the transfer function from w to z by H_{wz}, the inequality $\|H_{wz}\|_\infty^2<\mu$ holds if, and only if, there exists a symmetric matrix P such that

$$\begin{bmatrix}P & A_{CL}(K)P & B_1 & 0\\ PA_{CL}^T(K) & P & 0 & PC_{CL}^T(K)\\ B_1^T & 0 & I & D_{11}^T\\ 0 & C_{CL}(K)P & D_{11} & \mu I\end{bmatrix}\succ 0 \tag{46}$$

is feasible (De Oliveira, Geromel, & Bernussou, 2002). The optimal feedback controller K for the closed-loop system (45) is formulated as the optimization of the bilinear matrix inequality (BMI)

$$\min_{\mu,P,K}\ \mu\quad\text{subject to (46)}, \tag{47}$$

where $P=P^T\in\mathbb{R}^{n\times n}$ and $K\in\mathbb{R}^{1\times 2}$. The BMI (47) was solved using the PENBMI software (Kočvara & Stingl, 2006) as a MATLAB function in conjunction with the YALMIP (Lfberg, 2004) programming interface to find the fixed $\mathcal{H}_\infty$ controller $K=[1.8260\ 0.3205]$.

References

Alfieri, E., Amstutz, A., & Guzzella, L. (2009). Gain-scheduled model-based feedback control of the air/fuel ratio in diesel engines. *Control Engineering Practice*, *17*(12), 1417–1425 . doi:10.1016/j.conengprac.2008.12.008.

Apkarian, P., & Adams, R. J. (1998). Advanced gain-scheduling techniques for uncertain systems. *IEEE Transactions on Control Systems Technology*, *6*(1), 21–32.

Apkarian, P., Gahinet, P., & Becker, G. (1995). Self-scheduled $\mathcal{H}_\infty$ control of linear parameter-varying systems: A design example. *Automatica*, *31*(9), 1251–1261.

Balas, G., Doyle, J., Glover, K., Packard, A., & Smith, R. (2001). $\mu-$Analysis *and synthesis toolbox. Users Guide*. South Natick, MA: The MathWorks Inc.

Balluchi, A., Benvenuti, L., di Benedetto, M. D., Pinello, C., Sangiovanni-Vincentelli, A. L., & Parades, R. (2000). Automotive engine control and hybrid systems: Challenges and opportunities. *Proceedings of the IEEE*, *88*(7), 888–912.

Benninger, N., & Plapp, G. (1991). *Requirements and performance of engine management systems under transient conditions*. SAE 910083.

Caigny, J., Camino, J., Oliveira, R., Peres, P., & Swevers, J. (2008). Gain scheduled H_∞- control of discrete-time polytopic time-varying systems. In *Proceedings of conference on decision and control* (pp. 3872–3877).

Cassidy, J., Jr., & Athans, M. (1980). On the design of electronic automotive engine controls using linear quadratic control theory. *IEEE Transactions on Automatic Control*, *25*(5), 901–912.

Choi, S., Hedrick, J., Kelsey-Hayes, V., & Livonia, M. (1998). An observer-based controller design method for improving air/fuel characteristics of spark ignition engines. *IEEE Transactions on Control Systems Technology*, *6*(3), 325–334.

De Oliveira, M. C., Geromel, J. C., & Bernussou, J. (2002). Extended H_2 and H_∞ norm characterizations and controller parametrizations for discrete-time systems. *International Journal of Control*, *75*(9), 666–679.

Gahinet, P. (1996). Explicit controller formulas for LMI-based H_∞ synthesis. *Automatica*, *32*(7), 1007–1014.

Gahinet, P., Nemirovski, A., Laub, A., & Chilali, M. (1995). *LMI control toolbox—for use with Matlab.1995. Users Guide*. South Natick, MA: The MathWorks Inc.

Genç, A. U. (2002). *Linear parameter-varying modelling and robust control of variable cam timing engines*. Ph.D. thesis, University of Cambridge.

Heywood, J., Cohn, D., & Bromberg, L. (2007). Optimized fuel management system for direct injection ethanol enhancement of gasoline engines. *US Patent 7,225,787*, June 5.

Ikoma, T., Abe, S., Sonoda, Y., Suzuki, H., Suzuki, Y., & Basaki, M. (2006). *Development of V-6 3.5-liter engine adopting new direct injection system* SAE 2006-01-1259 2016 (p. 293).

Kočvara, M., & Stingl, M. (2006). PENBMI User's guide (Version 2.1). URL ⟨http://www.penopt.com⟩.

Lfberg, J. (2004). Yalmip: A toolbox for modeling and optimization in MATLAB. In *Proceedings of the CACSD conference*, Taipei, Taiwan. URL ⟨http://control.ee.ethz.ch/∼joloef/yalmip.php⟩.

Nagamune, R., & Choi, J. (2010). Parameter reduction of estimated model sets for robust control. *Journal of Dynamic Systems, Measurement, and Control*, *132*(2).

Onder, C. (1993). *Model-based multivariable speed and air-to-fuel ratio control of an SI engine*. SAE 930859.

Powers, W.E., Powell, B.K., & Lawson, G.P. (1983). Applications of optimal control and Kalman filtering to automotive systems. *International Journal of Vehicle Design SP4*. Applications of control theory in the automotive industry, 39–53.

Rivard, J. (1973). *Closed-loop electronic fuel injection control of the internal-combustion engine*. SAE 730005.

Skogestad, S., & Postlethwaite, I. (2005). *Multivariable feedback control: Analysis and design* (2nd ed.). New York: Wiley.

Suzuki, K., Shen, T., Kako, J., & Oguri, Y. (2007). Individual A/F control with fuel-gas ratio estimation for multi-cylinder IC engines. In *Proceedings of American control conference* (pp. 5094–5099).

Trefethen, L., & Bau, D. (1997). Numerical linear algebra. Society for Industrial and Applied Mathematics.

Wang, S. W., Yu, D. L., Gomm, J. B., Page, G. F., & Douglas, S. S. (2006). Adaptive neural network model based predictive control for air-fuel ratio of SI engines. *Engineering Applications of Artificial Intelligence*, *19*, 189–200.

Warren, J., Schaefer, S., Hirani, A. N., & Desbrun, M. (2007). Barycentric coordinates for convex sets. *Advances in Computational Mathematics*, *27*(3), 319–338.

Wu, F., & Dong, K. (2006). Gain-scheduling control of LFT systems using parameter-dependent Lyapunov functions. *Automatica*, *42*(1), 39–50.

Yildiz, Y., Annaswamy, A., Yanakiev, D., & Kolmanovsky, I. (2010). Spark ignition engine fuel-to-air ratio control: An adaptive control approach. *Control Engineering Practice*, *18*(12), 1369–1378.

Zhou, K., Doyle, J. C., & Glover, K. (1996). *Robust and optimal control*. Upper Saddle River, NJ: Prentice-Hall.